The effect of impurities on the R-point instability in $KMnF_3$. I. An X-ray scattering study

1989 J. Phys.: Condens. Matter 1 3565

(http://iopscience.iop.org/0953-8984/1/23/002)

J. Phys.: Condens. Matter 1 (1989) 3565–3577. Printed in the UK

The effect of impurities on the R-point instability in $KMnF_3$: I. An x-ray scattering study

U J Cox†
Department of Physics, University of Edinburgh, Mayfield Road, Edinburgh, UK

Received 1 September 1988

Abstract. The wavevector dependence of the critical fluctuations at the cubic-to-tetragonal structural phase transition in $KMnF_3$ doped with 1% and 10% of $KMgF_3$ has been studied using x-ray scattering techniques. It is found that the introduction of impurities lowers T_c and that the fluctuation-driven first-order transition becomes continuous when the impurity concentration exceeds a certain threshold. At temperatures far above T_c, the temperature dependence of the x-ray critical scattering cross section measured in the samples $KMnF_3$, $KMn_{0.99}Mg_{0.01}F_3$ and $KMn_{0.9}Mg_{0.1}F_3$ is described by the same critical exponents ν and γ. Contrary to expectation, the magnitude of the anomalous narrow component observed in the critical scattering in pure $KMnF_3$ close to T_c is significantly reduced by the introduction of the impurities.

1. Introduction

Despite considerable experimental and theoretical effort, the effect of impurities on structural phase transitions is still not fully understood. $KMnF_3$ undergoes a phase transition from a cubic to a tetragonal phase at a temperature of 186 K which has been studied in some detail (Minkiewicz *et al* 1970, Gesi *et al* 1972, Shapiro *et al* 1972, Nicholls and Cowley 1987 (hereafter referred to as I)). The present work is an experimental investigation of the transition in two crystals of $KMnF_3$ containing known proportions of the compound $KMgF_3$. This paper reports the results of x-ray scattering experiments, and a companion paper describes neutron scattering measurements (Cox and Cussen 1989).

$KMnF_3$ belongs to the family of perovskite crystals containing $SrTiO_3$ which undergo an antiferrodistortive phase transition driven by an instability of the high-temperature cubic phase against the R_{25} optic mode of vibration. The distorted phase has a unit cell which is double that of the cubic phase, since the unstable mode consists of alternating anti-phase rotations of the fluorine octahedra. The transition is characterised by a three-component order parameter with wavevector $\boldsymbol{q}_s = 2\pi/a_0\,(\frac{1}{2}, \frac{1}{2}, \frac{1}{2})$ and so might be expected to have a continuous phase transition described by the $n = d = 3$ Heisenberg model. Previous experimental work indicates that the transition is not continuous, and this is thought to occur because the critical fluctuations are strongly two-dimensional and drive the transition to be first order (Fossheim 1984, Natterman 1976). As reported in an earlier paper (Cox *et al* 1988 (hereafter referred to as II)), substitutional impurities

† Present address: Department of Physics, University of Durham, Durham, UK.

0935-8984/89/233565 + 13 $02.50

change the charcter of the transition and, above a small threshold concentration, the transition is continuous.

The classical soft-mode approach to the dynamical behaviour of a system undergoing a structural phase transition predicts that the spectral response can be characterised by a softening resonance with one associated timescale. However, neutron scattering measurements of the dynamic critical behaviour close to T_c by Riste *et al* (1971) on $SrTiO_3$ and Shapiro *et al* (1972) on $SrTiO_3$ and $KMnF_3$ revealed a resolution-limited component in the scattering profile centered on zero frequency in addition to the expected phonon-like contribution, indicating that the critical fluctuations occur on two distinct timescales. The first is relatively short and is set by the soft-mode side-band, while the second is a longer timescale associated with the narrow 'central peak'. This central peak has been attributed to the presence of impurities, as described in detail by Halperin and Varma (1976). Similarly, recent x-ray scattering measurements of the static critical response close to T_c in $SrTiO_3$, $RbCaF_3$ and $KMnF_3$ have revealed behaviour inconsistent with classical intrinsic theories, the scattering profile again comprising an anomalous second peak superimposed upon the phonon cross section and narrower in wavevector (Andrews 1986, Ryan *et al* 1986, I, Gibaud *et al* 1987a, b). This implies that the critical fluctuations occur on two length scales, the shorter being associated with the softening phonon and the longer corresponding to the anomalous component. Moreover, the longer length scale has been attributed to the presence of impurities, as qualitatively predicted by Imry and Wortis (1979).

The relationship between the central peak observed in neutron scattering experiments and the anomalous component observed in x-ray scattering experiments is of interest since although the two features are not immediately comparable, they may be manifestations of a common physical mechanism. The work presented here, and in the companion paper (Cox and Cussen 1989), attempts to correlate the two phenomena and also to further clarify the effect of impurities on a displacive structural phase transition.

2. Experimental arrangement

The measurements were performed in the extended face geometry on a triple-crystal x-ray diffractometer as described for work on $KMnF_3$ (I) and $RbCaF_3$ (Ryan *et al* 1986, Gibaud *et al* 1987a, b). Cu $K_{\alpha 1}$ radiation was produced by a rotating-anode generator operating at 3 kW with a focal spot size of 3×0.03 mm^2, and collimated by reflection from either a flat pyrolitic graphite (0 0 0 2) or a flat silicon (1 1 1) monochromator crystal. Similar analyser crystals were used to collimate the radiation scattered from the sample. With pyrolitic graphite monochromator and analyser crystals in position, the wavevector resolution in the scattering plane was $\sim 0.02(2)$ Å^{-1} and $\sim 0.007(2)$ Å^{-1} (FWHM) perpendicular and parallel to the scattered wavevector respectively. With silicon optics, this was reduced to $\sim 0.001(2)$ Å^{-1} in both directions in the plane. Perpendicular to the scattering plane, the resolution was limited by a slit to $\sim 0.05(1)$ Å^{-1} in both cases.

3. Sample preparation

The crystals $KMn_{0.99}Mg_{0.01}F_3$ and $KMn_{0.9}Mg_{0.1}F_3$ were grown by Dr R C C Ward of the Crystal Growth Facility at the University of Oxford. The size of the $KMn_{0.99}Mg_{0.01}F_3$ crystal was $\sim 8 \times 8 \times 9$ mm^3 and of the $KMn_{0.9}Mg_{0.1}F_3$ crystal was $\sim 10 \times 10 \times 15$ mm^3.

The samples for x-ray work were cut perpendicular to a crystallographic ⟨001⟩ direction from the grown crystals and consisted in each case of a slice ~2 mm thick. (The remainder of the grown crystals provided samples for the neutron scattering experiments described in Cox and Cussen (1989).) The active surface of the slices was polished and then etched for ten minutes in ortho-phosphoric acid to remove any surface damage.

The quality of the sample crystals was assessed by measuring rocking curve widths in the high-resolution configuration, and the mosaic spread was found in each case to be ~0.019(3)°. The samples were mounted in turn onto the cold finger of a closed-cycle cryostat in a strain-free manner, and oriented with the face normal [001] and a cubic [110] axis in the horizontal plane of the diffractometer, so as to observe scattering in the (1–10) plane. The temperature stability of the cryostat was ±0.02 K.

4. Theory of critical scattering

X-rays have a wavelength comparable with the lattice spacing of a crystal, but an energy considerably greater than typical phonon energies. Consequently, the measured scattering cross section automatically integrates over the energy to give the differential cross section $d\sigma/d\Omega$. In the one-phonon approximation for wavevector transfer $\boldsymbol{Q}$, in the neighbourhood of the R-point, the scattering is

$$\frac{d\sigma}{d\Omega} = S_1(\boldsymbol{Q}) = k_B T \sum_{ij} F_i(\boldsymbol{Q}) \chi_{ij}(\boldsymbol{q}) F_j(-\boldsymbol{Q}) \delta(\boldsymbol{Q} + \boldsymbol{q} - \boldsymbol{\tau}_R) \tag{1}$$

where $\chi_{ij}(\boldsymbol{q})$ is the static dielectric susceptibility and

$$F_j(\boldsymbol{Q}) = \sum_k f(k) \boldsymbol{Q} \cdot \boldsymbol{e}(k, \boldsymbol{q}_j) \exp[+i(\boldsymbol{Q} + \boldsymbol{q}) \cdot \boldsymbol{R}_k] \exp(-W_k) \tag{2}$$

is the structure factor of the normal mode j, with eigenvector $\boldsymbol{e}(k, \boldsymbol{q}_j)$. The sum runs over all atomic sites $\boldsymbol{R}_k$ in the unit cell, $f(k)$ being the form factor and $\exp(-W_k)$ the Debye-Waller factor for the kth atom. It is assumed that only the R_{25} mode is temperature-dependent and that all other modes contribute to a constant background. The structure factors for the phonon modes corresponding to rotations of the fluorine octahedra about the three cubic axes x, y and z for wavevectors in the (1–10) plane are $F_x(\boldsymbol{\tau}_R) = F_y(\boldsymbol{\tau}_R) = F$, and $F_z(\boldsymbol{\tau}_R) = 0$, so the x-rays couple equally to rotations about x and y only.

The wavevector dependence of the static susceptibility can be expanded as a Taylor series in $\boldsymbol{q}$. The coefficients of the quadratic terms which depend upon the direction of $\boldsymbol{q}$ may be reduced by symmetry for $KMnF_3$ (Cowley 1980) so that

$$\chi_{ij}^{-1}(\boldsymbol{q}) = [\chi_{ij}^{-1}(0)/\kappa^2](\kappa^2 + \boldsymbol{q}^2 + f\boldsymbol{q}_i^2)\delta_{ij} + h\boldsymbol{q}_i \cdot \boldsymbol{q}_j(1 - \delta_{ij}) \tag{3}$$

where $\boldsymbol{\kappa}$ is the inverse correlation length for the fluctuations, and f and h are measures of the anisotropy. These parameters have been estimated using neutron scattering by Gesi *et al* (1972) as $f = -0.99 \pm 0.01$ and $h = 0.14 \pm 0.04$. The critical scattering is therefore Lorentzian in wavevector, and extremely anisotropic.

The temperature dependence of the static susceptibility at $\boldsymbol{q} = 0$, and of the inverse correlation length are described by the equations

$$\begin{aligned} \chi_L &= \chi_{ij}(0) = C_+ t^{-\gamma_L} \\ \kappa_L &= \kappa_0 t^{\nu_L} \end{aligned} \tag{4}$$

where $t = (T/T_c - 1)$, $\kappa_0 = 2\pi/\xi_0$ and the subscript refers to a Lorentzian model.

As described in § 1, at temperatures close to T_c the x-ray critical scattering cross section in $KMnF_3$ contains an anomalous component that is significantly narrower than the scattering from the softening phonon. This component was analysed using a Lorentzian-squared functional form for the cross section, as expected for scattering from isolated symmetry-breaking defects which produce random static fields (Halperin and Varma 1976);

$$S_2(\boldsymbol{Q}) \propto c \sum_{\boldsymbol{q}} \chi^2(\boldsymbol{q})\delta(\boldsymbol{Q} + \boldsymbol{q} - \boldsymbol{\tau}_R) \tag{5}$$

where c is the concentration of impurities and $\chi(\boldsymbol{q})$ is assumed to be an isotropic susceptibility.

5. Experimental results

5.1. Measurement of T_c

In pure $KMnF_3$, the transition temperature was determined by an abrupt splitting of the (0 0 4) reciprocal lattice reflection into several tetragonal peaks within the temperature range $T = (187.6–187.4)$ K, measured using the high-resolution configuration (silicon monochromator and analyser crystals). In the disordered crystals the behaviour was less straightforward, so a comparison between studies of the (0 0 4) Bragg reflection and the temperature dependence of the integrated intensity of the (0.5 0.5 3.5) superlattice reflection (the primary order parameter) was made in each case. In $KMn_{0.99}Mg_{0.01}F_3$, the (0 0 4) reflection shifted along the [0 0 1] axis at a temperature of 183.9(2) K, but did not split into tetragonal peaks until a lower temperature of 182.4(2) K. Since the higher temperature coincided with a sudden change in the primary order parameter as shown in figure 1(*a*), this value is taken as T_c^1. A similar behaviour was observed in $KMn_{0.9}Mg_{0.1}F_3$ where new peaks were only clearly seen below a temperature of 159.0(5) K. However, a very small change in the lattice parameter occurred at 161.7(5) K, which coincided with the onset of long range order as shown in figure 1(*b*), so this value is taken as T_c^{10}. The effect of the impurities on the transition temperature has been discussed fully in a previous paper (II). The difference between the transition temperature T_c^{10} for $KMn_{0.9}Mg_{0.1}F_3$ and $T_c^0 = 187.5(1)$ K for $KMnF_3$ is approximately ten times the difference between the transition temperature T_c^1 for $KMn_{0.99}Mg_{0.01}F_3$ and T_c^0, as suggested by Rousseau *et al* (1975) and Kassan-Ogly and Nash (1986) using an argument based on atomic radii.

5.2. Measurement of the order parameter

The temperature dependence of the primary ($I(T)$) and secondary ($\eta = (c_t/a_t - 1)$) order parameters was measured in the disordered crystals, the former in a low-resolution configuration for two positions on each sample face and the latter in the high-resolution configuration, employing techniques described previously (I, II). The results are shown in figures 1 and 2, and each set was fitted independently by a least-squares technique to power laws of the form

$$\begin{aligned} I(T) &\propto (1 - T/T_c)^{2\beta} \\ \eta(T) &\propto (1 - T/T_c)^{2\dot{\beta}} \end{aligned} \tag{6}$$

where the transition temperature was allowed to vary to give T_c'. The resulting values

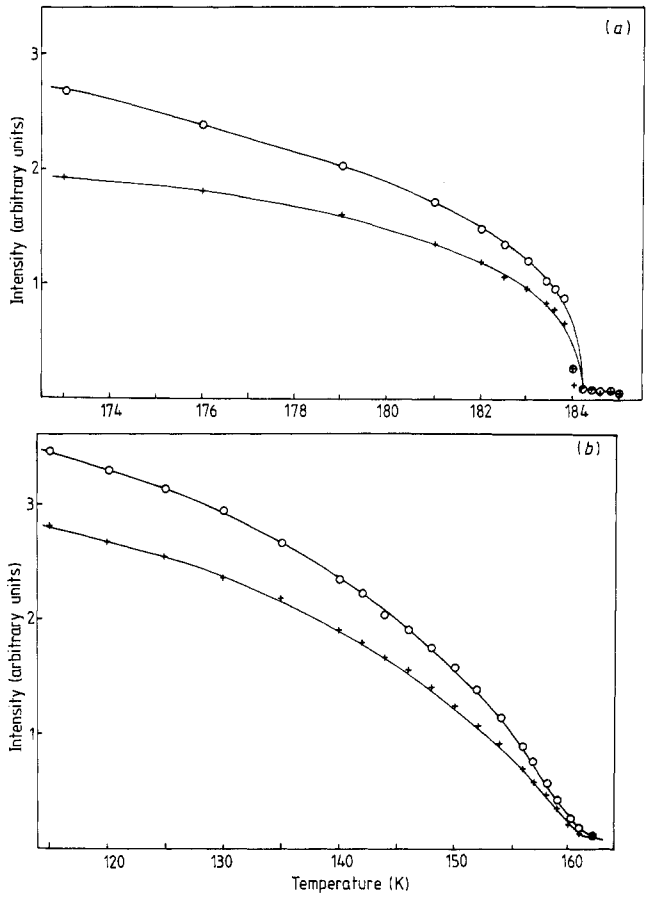

Figure 1. Integrated x-ray scattering intensity from the reciprocal lattice point (0.5 0.5 3.5) on $KMn_{1-x}Mg_xF_3$ obtained in a measurement of the rocking curve on cooling through T_c, for two different positions on the sample face (○ and +): (*a*) $x = 0.01$, and (*b*) $x = 0.1$. The smooth curves are fits to the upper power law (6) for the primary order parameter $I(T)$ as described in § 5.2.

for β and $\tilde{\beta}$ for the disordered crystals, together with the value for $\tilde{\beta}$ in $KMnF_3$ (I) are listed in table 1 and discussed in § 6. In $KMnF_3$ the temperature dependence of domain proportions meant that measurement of the integrated intensity at the R-point in reciprocal space did not give a reliable value for β, since at these positions in the (1–10) plane one of the tetragonal peaks is systematically absent. Measurements indicated that this is a less serious problem for the disordered crystals and that, contrary to pure $KMnF_3$, well below the transition temperatures all possible domains were present at various positions on the sample face. This demonstrates that the presence of impurities causes the sample to split into many small domains below T_c by nucleation.

The continuity of the phase transition in the pure and disordered crystals can be estimated from the fits in figure 2. The size of the first order step at T_c is $\sim 6.7 \times 10^{-4}$ for $KMnF_3$, $\sim 5.3 \times 10^{-4}$ for $KMn_{0.99}Mg_{0.01}F_3$ and ~ 0 for $KMn_{0.9}Mg_{0.1}F_3$, while measurements of the primary order parameter also suggest that in $KMn_{0.9}Mg_{0.1}F_3$ the transition is effectively continuous. This indicates that substitutional impurities alter the character

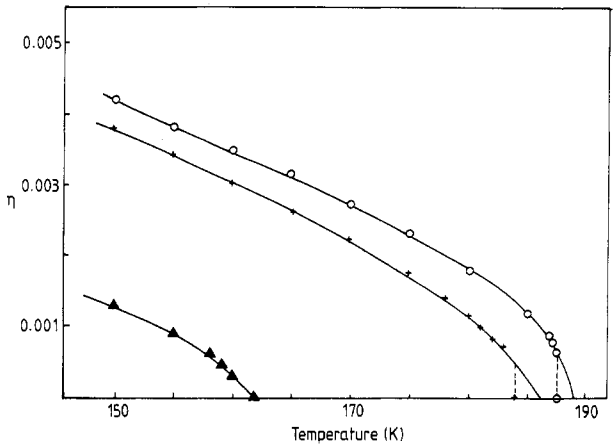

Figure 2. Temperature dependence of the secondary order parameter η $(=c_t/a_t - 1)$ for $KMn_{1-x}Mg_xF_3$: ○, $x = 0$; +, $x = 0.01$; ▲, $x = 0.1$. In each case the smooth curves are least-squares fits to the lower power law (6) described in § 5.2, and the dotted lines show the actual transition temperatures.

Table 1. Temperature dependence of the primary ($I(T)$) and secondary (η) order parameters in $KMn_{1-x}Mg_xF_3$, as given by least squares fitting of the data to the power laws (6). Errors are shown in brackets.

x	Plot	Figure/data	T_c' (K)	β or $\tilde{\beta}$
0.01	$I(T)$	1(*a*) ○	184.2 (0.2)	0.166 (0.010)
		+	184.2 (0.2)	0.123 (0.016)
	$\eta(T)$	2 +	186.5 (0.2)	0.336 (0.016)
0.1	$I(T)$	1(*b*) ○	161.1 (0.1)	0.298 (0.020)
		+	161.2 (0.1)	0.305 (0.024)
	$\eta(T)$	2 ▲	161.5 (0.2)	0.332 (0.020)
0	$\eta(T)$	2 ○	188.6 (0.07)	0.26 (0.02)

of the transition, and that above a small threshold concentration the transition is continuous (see II).

5.3. Critical Scattering

5.3.1. Experimental measurements. The wavevector dependence of the critical scattering above T_c was measured near the zone-boundary using the high- and low-resolution configurations for the disordered crystals. Some examples of low-resolution scans along the $\langle 0.5 + \zeta,\ 0.5 + \zeta,\ 3.5\rangle$ direction are shown in figure 3. As in $KMnF_3$ (I), the scattering profiles have temperature dependent widths and amplitudes. At $T = (T_c + 5.5)$ K, the scattering profile of all three samples is very similar with comparable widths, the scattering being narrowest and weakest in $KMnF_3$. By $T = (T_c + 0.3)$ K, however, the scattering cross section has changed considerably in $KMnF_3$, less so in $KMn_{0.9}Mg_{0.1}F_3$ and hardly at all in $KMn_{0.99}Mg_{0.01}F_3$. This is primarily reflected in the different values of the widths at this reduced temperature, which are ~0.008 RLU in $KMnF_3$, ~0.019 RLU

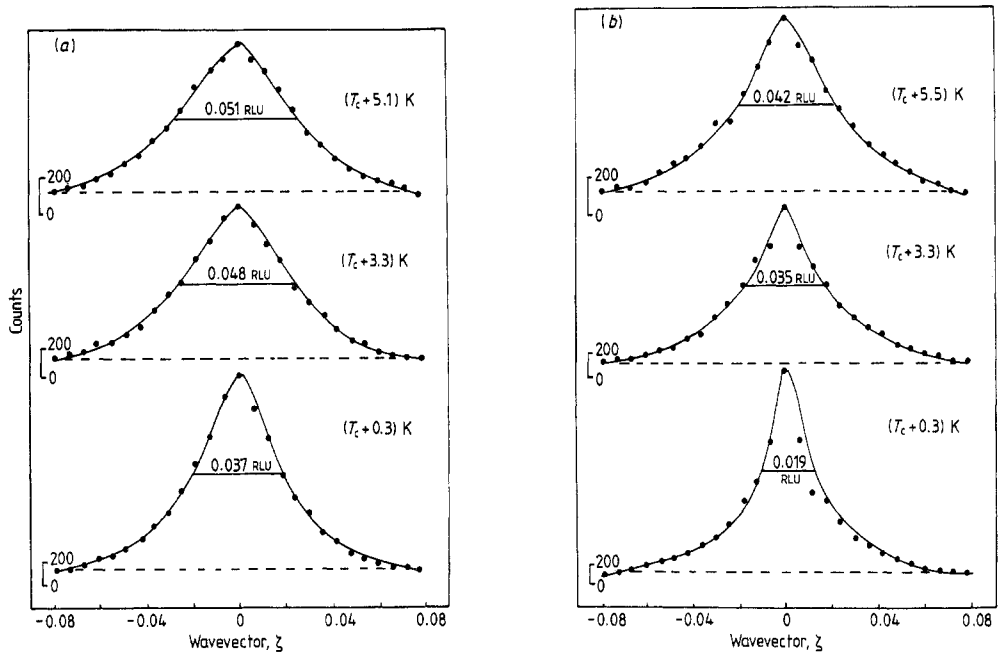

Figure 3. The diffuse x-ray scattering from $KMn_{1-x}Mg_xF_3$ obtained over one minute using the low-resolution configuration for wavevector $\boldsymbol{Q} = (0.5 + \zeta,\ 0.5 + \zeta,\ 3.5)$ at various temperatures above T_c for (*a*) $x = 0.01$, and (*b*) $x = 0.1$. The curves are least-squares fits to the model scattering function $S_1(\boldsymbol{Q}) + S_2(\boldsymbol{Q})$ convolved with the instrumental resolution function.

in $KMn_{0.9}Mg_{0.1}F_3$ and ~0.037 RLU in $KMn_{0.99}Mg_{0.01}F_3$, the intensity of the scattering being nominally the same in all three samples.

The scattering cross section measured in the high resolution configuration contains only the narrow anomalous component, the soft phonon being indistinguishable from a uniform background. Scans were obtained in the directions $\langle 0.5 + \zeta,\ 0.5 + \zeta,\ 2.5\rangle$ and $\langle 0.5\ 0.5\ 2.5 + \zeta\rangle$ for the disordered crystals above T_c, but the scattering was very weak. The peak widths were greater than the instrumental resolution in both samples, but any temperature dependence was less pronounced than in the case of pure $KMnF_3$ (I): below T_c the width of the scattering was limited by the resolution of the instrument.

5.3.2. Analysis of results. Pairs of scans with wavevector $\langle 0.5 + \zeta,\ 0.5 + \zeta,\ 3.5\rangle$ and $\langle 0.5, 0.5, 3.5 + \zeta\rangle$ obtained with the low-resolution configuration at various temperatures were fitted simultaneously to the model scattering function $S_1(\boldsymbol{Q})$ convolved with the instrumental response function. The anisotropy parameters were fixed at $f = -1$ and $h = 0$ as for $KMnF_3$ (I), the amplitude χ_L and inverse correlation length κ_L being varied with a fixed background. For $KMn_{0.99}Mg_{0.01}F_3$, this model continued to give reasonable fits over the whole temperature range, though when an additional model scattering function $S_2(\boldsymbol{Q})$ (with amplitude χ_{L^2} and inverse correlation length κ_{L^2}) was introduced for temperatures very close to T_c, the fits did improve slightly. For $KMn_{0.9}Mg_{0.1}F_3$, the fits for temperatures $\sim(T_c + 2)$ K and below were improved with the inclusion of an isotropic Lorentzian-squared component in the scattering model. The values of the four parameters κ_L, κ_{L^2}, χ_L and χ_{L^2} obtained from the fits for both

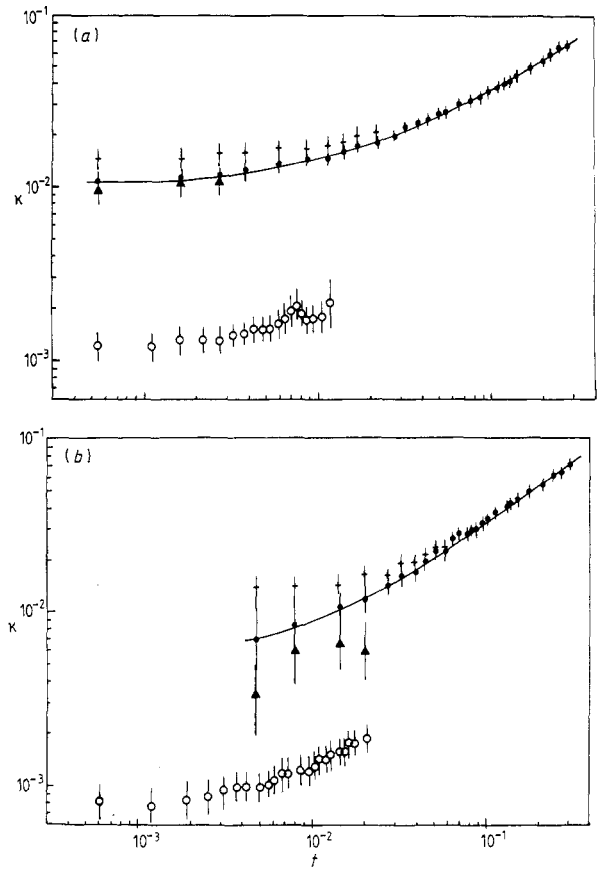

Figure 4. Inverse correlation lengths obtained from the analysis described in § 5.3.2 of the diffuse x-ray scattering for $KMn_{1-x}Mg_xF_3$ (in units of $2\pi/a_0$) for the reciprocal lattice points (0.5 0.5 3.5) (●, + and ▲) and (0.5 0.5 2.5) (○). (*a*) $x = 0.01$, and (*b*) $x = 0.1$. ● correspond to low-resolution data analysed using model $S_1(\boldsymbol{Q})$ only (to give κ_L). + and ▲ refer to the same data analysed using model $S_1(\boldsymbol{Q}) + S_2(\boldsymbol{Q})$, + to κ_L and ▲ to $\kappa_L{}^2$. ○ refer to the high-resolution data, analysed with model $S_2(\boldsymbol{Q})$ only to give $\kappa_L{}^2$. (S_2) The full curves are least-squares fits to the power law discussed in the text.

samples are shown in figures 4 and 5 as functions of the reduced temperature. The full curves are least-squares fits to the power laws given in equations (4) with the transmission temperature allowed to vary to give T_c'. The values of the critical exponents ν_L and γ_L obtained are shown in table 2 and discussed in § 6.

The data collected with the high-resolution configuration for the disordered crystals were fitted to a model scattering function $S_2(\boldsymbol{Q})$ convolved with the instrumental response function. This gave values for the amplitude $\chi_L{}^2(S_2)$ and width $\kappa_L{}^2(S_2)$ which are shown in figures 4 and 5: their magnitude and temperature dependence will be discussed in conjunction with the results for $KMnF_3$ in § 6.

5.3.3. The temperature dependence and amplitude of the anomalous component. The weightings of the Lorentzian and Lorentzian-squared components obtained from the analysis of the low-resolution critical scattering cross section are shown in figure 6

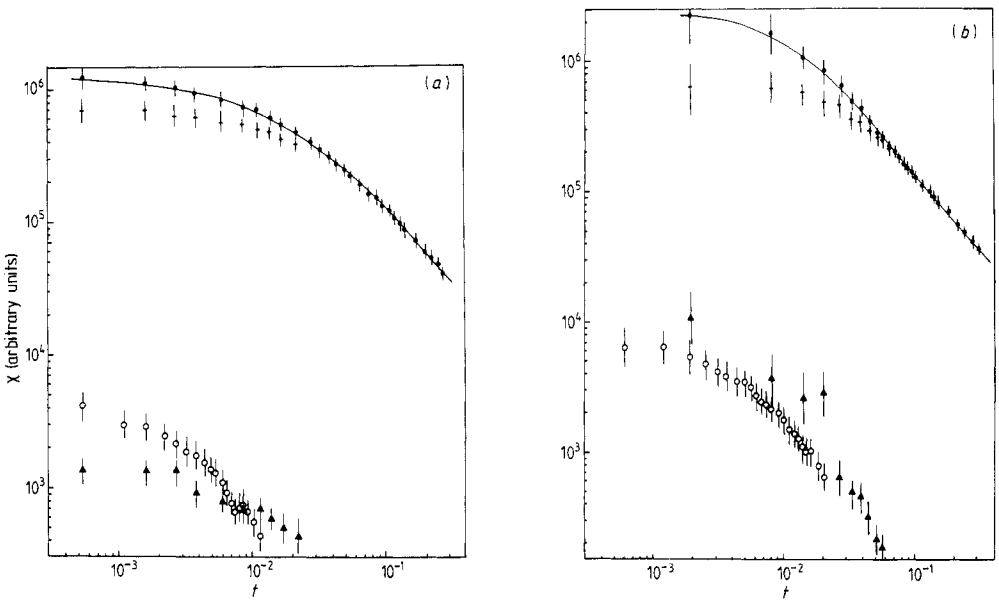

Figure 5. Amplitude obtained from the analysis as described in § 5.3.2 of the diffuse x-ray scattering for from $KMn_{1-x}Mg_xF_3$ the reciprocal lattice points (0.5 0.5 3.5) (●, + and ▲) and (0.5 0.5 2.5) (○) for (*a*) $x = 0.01$, and (*b*) $x = 0.1$. ● correspond to the low-resolution data analysed with model $S_1(\boldsymbol{Q})$ only (to give χ_L). + and ▲ refer to the same data analysed using model $S_1(\boldsymbol{Q}) + S_2(\boldsymbol{Q})$ (+ to χ_L and ▲ to $\chi_L{}^2$). ○ correspond to the high-resolution data analysed with model $S_2(\boldsymbol{Q})$ only (to give $\chi_L{}^2(S_2)$). The full curves are least squares fits to the power law discussed in the text.

Table 2. Critical exponents of the Lorentzian component obtained by least-squares fitting of the data in figures 4 and 5 to power laws (4) for $KMn_{1-x}Mg_xF_3$. Errors are shown in brackets.

x	ν_L	$\xi_L(T = T_c + 1)$ K Å	$T_c' - T_c$(K)	γ_L	$T_c' - T_c$(K)
0.01	0.65 (0.08)	480 (90)	−3.4 (1.0)	1.19 (0.15)	−3.1 (1.0)
0.1	0.74 (0.05)	830 (160)	−1.4 (1.0)	1.59 (0.17)	−2.8 (0.7)
0	0.62 (0.07)	740 (150)	—	1.19 (0.11)	—
Theory for $n = d = 3$ model	0.705 (0.003)	—	—	1.386 (0.004)	—

for the three samples $KMnF_3$, $KMn_{0.99}Mg_{0.01}F_3$ and $KMn_{0.9}Mg_{0.1}F_3$ as a function of temperature. For the disordered crystals there is a cross-over temperature of $\sim(T_c + 2)$ K for $KMn_{0.99}Mg_{0.01}F_3$ and $\sim(T_c + 5)$ K in $KMn_{0.9}Mg_{0.1}F_3$. In pure $KMnF_3$ the anomalous scattering contribution dominates from ~8 K above T_c and is relatively more intense than in either of the disordered samples.

Figure 7 is a plot of the temperature dependence of the temperature over the peak intensity (unprocessed data) of the R-point scattering collected at the reciprocal lattice point (0.5 0.5 2.5) in the high-resolution configuration, for the disordered crystals above the transition. The data is normalised to a counting time of one minute, and was collected with the x-ray spectrometer in identical configurations for both samples. Since the x-ray

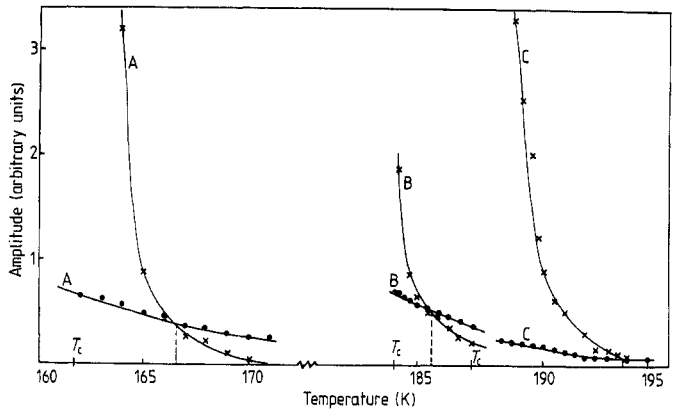

Figure 6. The relative weighting of the two components $S_1(Q)$ and $S_2(Q)$ in the analysis of the x-ray data collected in the low-resolution configuration for all three samples of $KMn_{1-x}Mg_xF_3$, as a function of temperature. In each case, ● refer to $S_1(Q)$ and × to $S_2(Q)$. The broken lines show the cross-over temperatures. Curves A, $x = 0.1$; curves B, $x = 0.01$; curves C, $x = 0$.

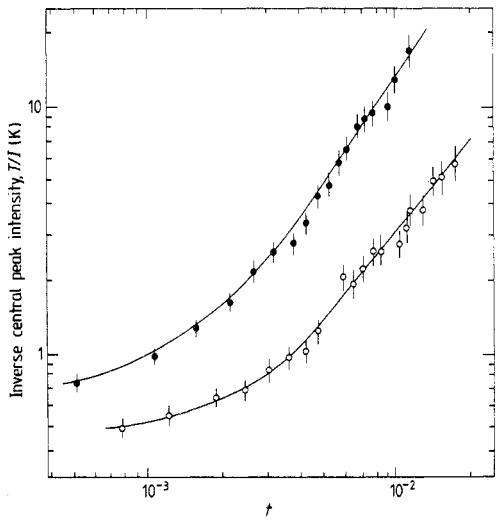

Figure 7. Temperature over the observed peak intensity of the x-ray scattering (measured in the high-resolution configuration and normalised to a counting time of 1 min) at the reciprocal lattice point (0.5 0.5 2.5) for $KMn_{1-x}Mg_xF_3$ versus the reduced temperature above T_c. ●, $x = 0.01$; ○, $x = 0.1$.

beam illuminates only a small part of the sample, and the width of the scattering was only slightly greater than the resolution width in both cases, this figure gives a reasonable estimate of the relative intensities of the anomalous component observed in the two samples. It can be seen that the scattering above T_c in $KMn_{0.9}Mg_{0.1}F_3$ is consistently more intense than in $KMn_{0.99}Mg_{0.01}F_3$ and that the temperature dependence is similar in both. The unprocessed scattering intensity observed in pure $KMnF_3$ is not included on the graph since the experiment was performed at an earlier date when the incident x-ray beam may have been of different amplitude.

6. Discussion of results

6.1. Temperature dependence of the order parameter

The values of the critical exponents β and $\tilde{\beta}$ obtained from the analyses of the order parameter in the disordered crystals are shown in table 1. For $KMn_{0.99}Mg_{0.01}F_3$ the values of β are considerably smaller than the value of $\tilde{\beta}$. A similar behaviour was found in pure $KMnF_3$ (I) which is also a first-order transition and where the domain proportions were temperature dependent. For the same reasons only the value of $\tilde{\beta}$ is considered reliable for $KMn_{0.99}Mg_{0.01}F_3$. In the case of $KMn_{0.9}Mg_{01}F_3$ the values of β and $\tilde{\beta}$ agree within error, which suggests the temperature dependence of the domain proportions is minimal in this sample.

The values obtained for the critical exponent in the three materials are lower than predicted by the $n = d = 3$ Heisenberg model where $\beta = 0.365$ and $\tilde{\beta} = 0.425$ (Le Guillou and Zinn-Justin 1980, Aharony and Bruce 1974). This may be because the phase transition occurs in the vicinity of a tricritical point, where $\beta = \tilde{\beta} = 0.25$ (Chang *et al* 1974). However, our results indicate that the presence of substitutional impurities tends to increase the dependence of the order parameter upon temperature and to make the transition more continuous.

6.2. Critical scattering

6.2.1. Temperature dependence of the soft-phonon. The wavevector dependence of the critical scattering obtained with the low-resolution configuration in the disordered crystals was well described by an anisotropic Lorentzian function (with a $\boldsymbol{q}$-dependent width) over a large range of the temperatures investigated. The critical exponents γ_L and ν_L for the pure and disordered crystals are shown in table 2, together with the theoretically predicted parameters of the $n = d = 3$ Heisenberg model (Le Guillou and Zinn-Justin 1980). The values obtained for $KMn_{0.99}Mg_{0.01}F_3$ are very similar to those of pure $KMnF_3$, slightly smaller than predicted by the Heisenberg model. The values for $KMn_{0.9}Mg_{0.1}F_3$ are larger, suggesting that the correlation and amplitude of the fluctuations increase more rapidly as T_c is approached than in the other two samples: this is expected at a continuous phase transition where the fluctuations diverge. Also, the presence of an anomalous component in the scattering cross section close to T_c will affect the values for the critical exponents: examination of the magnitude of the susceptibility and inverse correlation length in the three samples for $t > 0.05$ ($T \geqslant (T_c + 8)$ K) shows them to be identical. This demonstrates that far above the transition the effect of the impurities upon the critical behaviour is minimal. The values for the correlation length at $(T_c + 1)$ K are of the same order of magnitude in the three samples, though slightly smaller in $KMn_{0.99}Mg_{0.01}F_3$.

In all fits the transition temperature was allowed to vary, producing an offset from the experimentally determined value. The offset is larger in $KMn_{0.99}Mg_{0.01}F_3$ than in $KMn_{0.9}Mg_{0.1}F_3$ for both χ_L and κ_L which implies that the transition is more first order for the former, in agreement with the result found by monitoring the tetragonal strain. In $KMnF_3$ the data collected at temperatures close to T_c could not be fitted unless an isotropic Lorentzian-squared component was included in the model scattering function; when this was done χ_L and κ_L were independent of temperature for $T < (T_c + 1.5)$ K, consistent with a first order phase transition. Hence the analysis of the critical scattering

data in the three samples further demonstrates that substitutional impurities alter the character of the phase transition.

6.2.2. The effect of impurities on the anomalous component in $KMnF_3$. The substitution of Mg impurity ions for Mn ions in $KMnF_3$ influences the wavevector width and the amplitude of the anomalous component. In all three samples the anomalous scattering measured with the high-resolution configuration above T_c was broader than the resolution limit and well described by an isotropic Lorentzian-squared function. The deconvolved values of the widths and amplitudes of the component in the disordered crystals are shown in figures 4 and 5, and can be compared with the results for $KMnF_3$ (I). At $T \sim (T_c + 0.3)$ K the width of the scattering is approximately the same in $KMnF_3$ and $KMn_{0.9}Mg_{0.1}F_3$ (corresponding to a correlation length of 5000–6000 Å) but larger in $KMn_{0.99}Mg_{0.01}F_3$ (corresponding to a correlation length of ~3500 Å) and is most intense in $KMnF_3$ and weakest in $KMn_{0.99}Mg_{0.01}F_3$ (this result is also shown in figure 6). The measurements suggest that a substitutional impurity does not tend to enhance the component, but rather to reduce it. Also, though the width and magnitude of the component are sample-dependent, they do not vary consistently with impurity content. The Lorentzian-squared model, which is a good description of our results, is appropriate when a system contains random fields. However, the impurities introduced here occur at symmetry conserving positions and so are more likely to produce random bonds than random fields. This may explain why the magnitude of the anamalous component changes inconsistently with the dopant concentration while displaying a variation between samples.

The temperature dependence of the anomalous peak in the disordered crystals is not easily reconciled with the explanation of the second length scale given previously (Ryan *et al* 1986, I, Gibaud *et al* 1987a, b): It was suggested that the component arises from large-scale defect mediated fluctuations into the tetragonal phase that diverge at T_c, as qualitatively predicted by Imry and Wortis (1979) for a first order phase transition involving random fields. In $KMnF_3$ the fluctuations diverge at the measured transition temperature, but in the disordered crystals the width and amplitude of the scattering saturate within one degree of the transition and the fluctuations undergo a first-order transition at T_c. These results do not support the idea that the transition assumes the character of a percolation transition, in which the tetragonally distorted clusters increase in size as T_c is approached and eventually encompass the entire crystal. Rather, the results suggest that the clusters formed in the disordered crystals play a relatively passive role in the transition.

Finally, we have found that substitutional impurities in $KMnF_3$ decrease the anomalous x-ray component rather than increase it, which may be because these impurities are more likely to introduce random bonds than random fields and an increase in the concentration of the latter could only occur as a secondary effect. Also, the presence of a second type of fluctuation in the system is contingent upon a first order phase transition, so the amplitude of the anomalous component might be expected to decrease as the phase transition becomes more continuous.

Acknowledgments

I am grateful to Dr R C C Ward for growing the crystals. I have benefited from helpful discussions with Professor R A Cowley, and from the technical support of Mr H Vass.

Financial support, including a studentship, was provided by SERC for which I am grateful.

References

Aharony A and Bruce A D 1974 *Phys. Rev. Lett.* **33** 427
Andrews S R 1986 *J. Phys. C: Solid State Phys.* **19** 3721
Chang T S, Tuthill G F and Stanley H E 1974 *Phys. Rev.* B **9** 4882
Cowley R A 1980 *Adv. Phys.* **29** 1
Cox U J and Cussen LD 1989 *J. Phys.: Condens. Matter* **1** 3579–89
Cox U J, Gibaud A and Cowley R A 1988 *Phys. Rev. Lett.* **61** 982
Fossheim, K 1984 *Multicritical Phenomena* vol 106 ed. R Pynn and A Skeltorp (Plenum ASI) p 129
Gesi K, Axe J D, Shirane G and Linz A 1972 *Phys. Rev.* B **5** 1933
Gibaud A, Ryan T W and Nelmes R J 1987a *J. Phys. C: Solid State Phys.* **20** 3833
Gibaud A, Cowley R A and Mitchell P W 1987b *J. Phys. C: Solid State Phys.* **20** 3849
Halperin B I and Varma C M 1976 *Phys. Rev.* B **14** 4030
Imry Y and Wortis M 1979 *Phys. Rev.* B **19** 3580
Kassan-Ogley F A and Nash V E 1986 *Acta Crystallogr.* B **42** 307
Le Guillou J C and Zinn-Justin J 1980 *Phys. Rev.* B **21** 3976
Minkiewicz V J, Fujii Y and Yamada Y 1970 *J. Phys. Japan* **28** 443
Natterman T 1976 *J. Phys. C: Solid State Phys.* **9** 3337
Nicholls U J and Cowley R A 1987 *J. Phys. C: Solid State Phys.* **20** 3417
Riste T, Samuelsen E J, Otnes K and Feder J 1971 *Solid State Commun.* **9** 1455
Rousseau M, Gesland J Y, Julliard J, Nouet J, Zarembovitch J and Zarembovitch A 1975 *Phys. Rev.* B **12** 1579
Ryan T W, Nelmes R J, Cowley R A and Gibaud A 1986 *Phys. Rev. Lett.* **56** 2704
Shapiro S M, Axe J D, Shirane G and Riste T 1972 *Phys. Rev.* B **6** 4332